

Drifting representation with transient resets characterizes sensorimotor transformation in the monkey superior colliculus

Michelle R. Heusser^{1,3}, Uday K. Jagadisan^{1,3}, Neeraj J. Gandhi¹⁻³

Departments of Bioengineering¹ and Neuroscience², and Center for the Neural Basis of Cognition³,
University of Pittsburgh, Pittsburgh, PA, USA.

1 ABSTRACT

2 To produce goal-directed eye movements known as saccades, we must channel sensory input from our
3 environment through a process known as sensorimotor transformation. The behavioral output of this
4 phenomenon (an accurate eye movement) is straightforward, but the coordinated activity of neurons
5 underlying it is not well understood. We searched for a neural correlate of sensorimotor transformation
6 in the activity patterns of simultaneously recorded neurons in the superior colliculus (SC) of rhesus
7 monkeys performing a standard delayed saccade task. Neurons in its intermediate layers produce a
8 burst of spikes both following the appearance of a visual (sensory) stimulus and preceding an eye
9 movement command, but many also exhibit a sustained activity level during the intervening time (“delay
10 period”). Each session’s population activity was summarized in a low-dimensional framework and
11 assessed on a scale of visual- to motor-like throughout the delay period using a novel measure we call
12 the Visuomotor Proximity Index (VMPI). On average, population activity slowly evolved from a more
13 visual- to a more motor-like pattern throughout the delay period, but microsaccade perturbations
14 transiently deviated it to a visual-like pattern. A correlation was also found between the VMPI and single
15 trial saccadic reaction time, even hundreds of milliseconds before the cue to initiate a movement.
16 Therefore, we conclude that SC population activity contains a neural signature of the sensorimotor
17 transformation process, systematically drifting toward a motor-like representation and intermittently
18 reverting to a visual-like representation following a microsaccade.

19 *Key words:* sensorimotor transformation, population activity, superior colliculus, state-space framework,
20 dimensionality reduction, saccade initiation, delayed saccade task

21

22 INTRODUCTION

23 Sensorimotor transformation is the framework by which our brains process sensory input and
24 subsequently produce a motor command. Its functionality is easily appreciated in the oculomotor
25 system – when we see an object in our periphery, we can promptly direct our line of sight to that target.
26 However, at what times are the neural populations representing the presence of a visual target through
27 their coordinated activity? At what times are they collectively producing a signal that more closely
28 resembles a motor command? And how does the population response transition from sensory to motor
29 representations?

30 The superior colliculus (SC) is a midbrain structure crucial for sensorimotor transformation (Basso and
31 May, 2017; Cooper and McPeck, 2021; Gandhi and Katnani, 2011; Sajad et al., 2020; Wurtz and
32 Optican, 1994). Neurons in its deeper layers emit strong bursts of activity both when a visual stimulus
33 appears as well as when a high-velocity eye movement, known as a saccade, is generated to redirect
34 gaze toward that object of interest. These putative “visual” and “motor” bursts are well characterized but
35 the time course of integrating visual stimulus-related information into a motor command is not
36 understood as well. Previous research on sensorimotor integration in the oculomotor system has relied
37 on single unit studies. These studies have focused on reference frame transformations, with the
38 objective of determining whether the temporally evolving neural activity better represents stimulus
39 location or movement amplitude. The general result is that, immediately after stimulus presentation, the
40 sensory response is encoded in the reference frame of the stimulus modality – oculocentric for vision
41 and craniocentric for audition. Just prior to the movement onset, the activity is best represented as a
42 motor command in eye-centered coordinates or in a hybrid reference frame. In the intervening delay
43 period, the average activity shows a slow and systematic transition from sensation to action
44 representations, one which is sped up when no delay period is imposed. Such findings have been
45 reported in the SC (Lee and Groh, 2012; Sajad et al., 2020; Sadeh et al., 2020), frontal eye fields
46 (Caruso et al., 2018b; Sajad et al., 2016), parietal cortex (Buneo et al., 2002; Mullette-Gillman et al.,

47 2005), and supplementary eye fields (Bharmuria et al., 2021). We sought to characterize at a
48 population level the moment-by-moment representation of SC activity between sensation and action.
49 We labeled the transient burst representations that follow target onset and precede saccade onset as
50 'visual' and 'motor' subspaces, respectively, while remaining agnostic to their preferred coordinate
51 system. We then sought to determine how the population activity during the delay period transitioned
52 between the two representations. This approach provides a more unsupervised yet still direct
53 understanding of how SC populations encode these features. To this end, we searched for a neural
54 correlate of sensorimotor transformation in small populations of SC neurons by characterizing the
55 “visual-like” or “motor-like” pattern of activity during the intervening period of time between the visual
56 and motor bursts while rhesus monkeys (*Macaca mulatta*) performed a visually-guided delayed
57 saccade task (Figure 1). This paradigm temporally separates the visual from the motor epoch through a
58 “delay period” and has been previously employed in countless studies of cognition, sensation, and
59 motor behavior.

60 To characterize the shared activity patterns of neural populations, machine learning methods such as
61 dimensionality reduction have been utilized to investigate the dynamics of neural activity underlying
62 cognitive or behavioral processes such as stimulus encoding (e.g., Cowley et al., 2016), decision
63 making (e.g., Aoi et al., 2020), and movement execution (e.g., Churchland et al., 2006). Such
64 techniques transform the activity across the population into a state-space framework, where the pattern
65 at any given moment can be represented as a linear combination of the activity of individual neurons.
66 This methodology offers a noise-reduced, better-visualizable trajectory of activity across consecutive
67 time points (Cunningham and Yu, 2014). Here, we employed a dimensionality reduction algorithm
68 called Gaussian Process Factor Analysis (GPFA, Yu et al., 2009), to characterize the time course of
69 population-level representations as they relate to vision and saccadic eye movement. First, we used a
70 linear discriminant analysis (LDA) classifier to determine if the “subspaces” formed by collective activity
71 patterns during the visual and motor epochs were distinguishable from each other and found that for
72 the bulk of neural populations, this was indeed the case. Exploiting this separability, we then computed
73 the similarity of the activity patterns throughout the delay period to either the visual or the motor
74 subspace through a Visuomotor Proximity Index (VMPI) (based on the proximity index in Dekleva et al.,
75 2018). When looking across repetitions of the task, activity patterns exhibited a slow, systematic drift
76 from a visual- to a motor-like pattern. Remarkably, whenever a microsaccade occurred during the delay
77 period, the population activity pattern transiently deviated to a visual-like representation before rapidly
78 returning to the original trajectory. Finally, we tested an existing theory of arm movement generation
79 known as the “initial condition hypothesis” (Afshar et al., 2011) and found that the state-space position
80 of the activity on a given trial was correlated with the eventual saccadic reaction time, a relationship that
81 emerged even hundreds of milliseconds before the cue to initiate a movement.

82 This study extends our knowledge of the SC's role in sensorimotor transformation through both a
83 network-level analysis of neural activity across sensorimotor epochs as well as a direct investigation of
84 the relationship between this intermediate activity and behavior. Taken all together, these findings
85 indicate that 1) there is a neural signature of the sensorimotor transformation process present in SC
86 populations that can be characterized by a slow drift with transient resets, and that 2) activity patterns
87 that drift to a stronger motor-like representation by the end of the delay period may enable a more rapid
88 initiation of a saccade, substantiating the idea that this movement initiation mechanism is conserved
89 across motor systems.

90

91 RESULTS

92 In this study, we aimed to characterize delay period activity as exhibiting a visual- or motor-like signal
93 and explored the relationship between this activity and the motor behavior to better understand the

94 neural correlates of sensorimotor transformation in the SC. Neural activity from small populations of
95 neurons was recorded simultaneously with multi-contact laminar probes traversing the dorsoventral
96 axis of the SC as rhesus monkeys performed a delayed saccade task (Figure 1A-B). Data are
97 examined from 27 recording sessions and limited to the subset of trials for which the visual stimulus
98 and subsequent saccade were directed near the center of the response field. For electrode
99 penetrations orthogonal to the SC surface, as we used here, all neurons recorded in a single session
100 have comparable response fields, and care was taken to drive the electrode to the intermediate layers
101 to capture mostly visuomotor neurons (i.e., those having both visual- and a motor-related increases in
102 activity). A 24-channel laminar electrode was used for 15 of the sessions and a 16-channel electrode
103 for the other 12 sessions. Spike sorting was performed and resulted in 12.3 (± 3.3 , range [7,19])
104 neurons per track, or population, on average. Across all 27 sessions, a total of 331 neurons were
105 recorded.

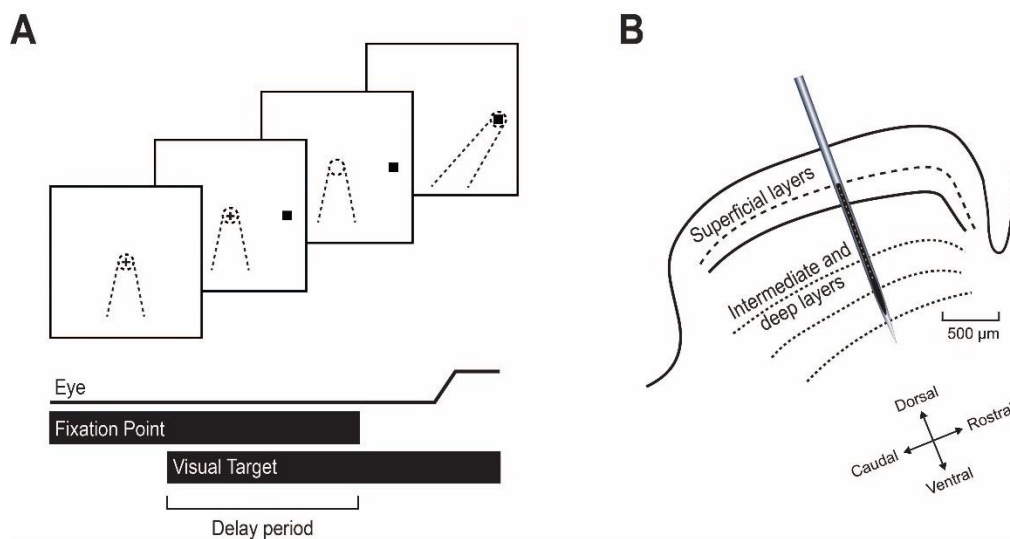


Figure 1. Schematic representation of behavioral task and neurophysiological preparation used in this study. A. Standard event sequence in the delayed saccade task. Top – The animal fixates on a central point (shown as a plus sign in this illustration). A target (black square) appears in the periphery for a variable “delay period.” The dynamics of sensorimotor transformation were analyzed during much of the delay period. The disappearance of the fixation point acts as the go cue to generate a saccade toward the target. Center of gaze is depicted in all snapshots as a dotted cone. Bottom – A typical timeline of key events in a single trial of this task. **B.** In each experiment, a linear multielectrode array with 16 or 24 recording contacts was acutely inserted orthogonal to the SC surface along the dorsoventral axis to obtain a neural population representation as monkeys performed the delayed saccade task. Figure adapted from Jagadisan & Gandhi, 2022.

106 **Visual and motor subspaces are separable**

107 We started by plotting for all contacts the average spike density profiles aligned on target and saccade
108 onsets. We also separated the delay period from the transient visual burst, as shown for one session in
109 Figure 2A. We then applied GPFA (Yu et al., 2009) to compute the latent activity patterns during these
110 epochs (Figure 2B). For most datasets (23/27), including this one, the top 3 factors accounted for at
111 least 95% percent of the variance in the spike density profiles (Figure 2D). Thus, we limited our
112 analysis to 3 dimensions, which also facilitated visualization. Moreover, instead of plotting the factors as
113 a function of time, the low-dimensional activity can be illustrated in a three-dimensional state space, in
114 which a single point denotes activity across the population taken from a 20 ms window from one trial
115 (Figure 2C). This framework, on which we base our first set of analyses, allows an assessment of the
116 regions, or “subspaces,” where the activity resides during the various epochs of the trial.

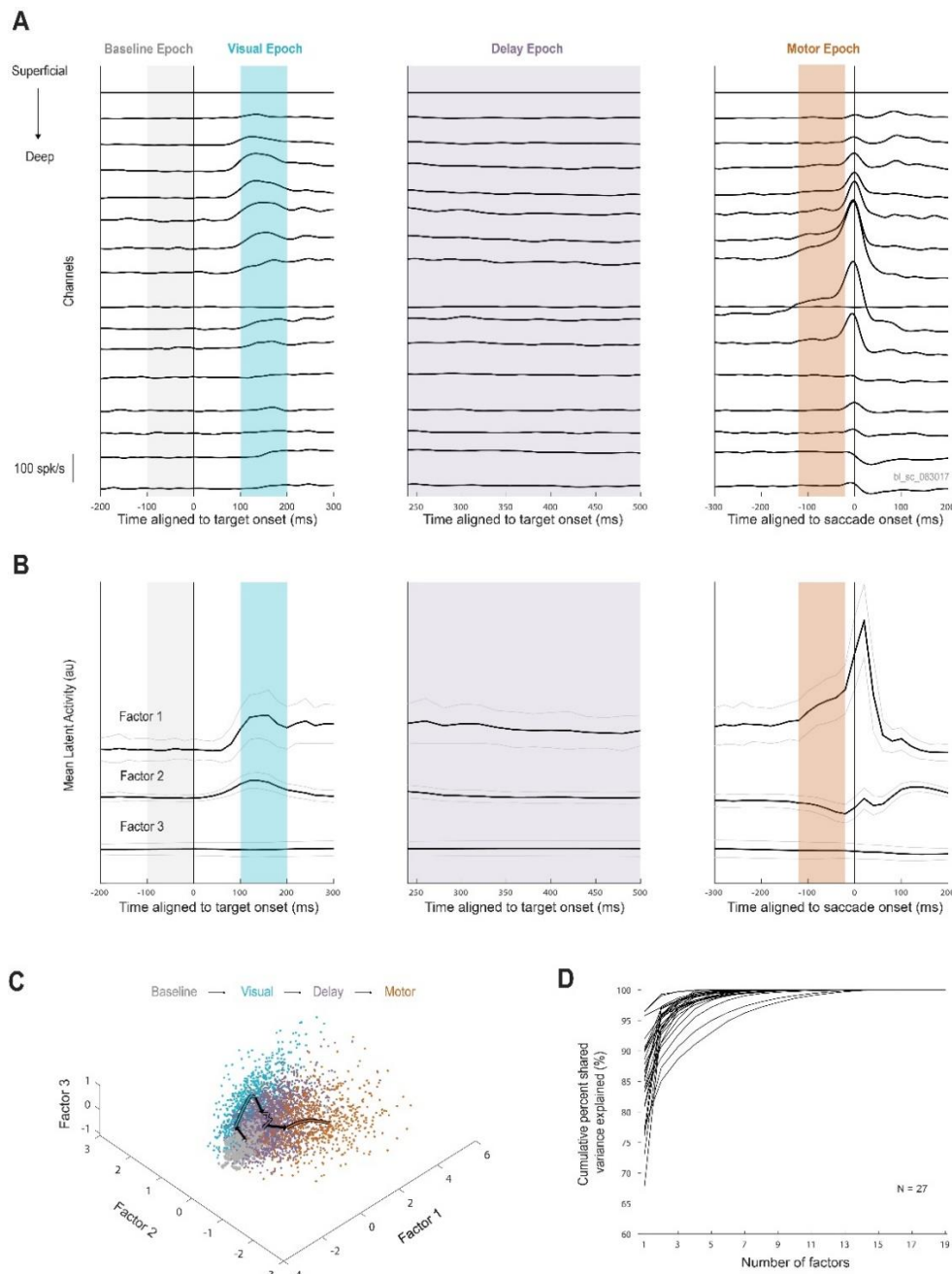


Figure 2. Analysis of neural population activity in a state space framework allows for an evaluation of subspace separability. **A.** Trial-averaged firing rates across electrode depth are shown for one example session. Multiunit activity on each of 16 channels is plotted aligned to target onset (left and middle) or saccade onset (right). Each epoch window is defined by a vertical rectangle (baseline in gray, visual in cyan, delay in purple, and motor in orange). Delay period activity was defined to start 240 ms after target onset, by which time the transient visual response had subsided. **B.** Latent population activity after dimensionality reduction using Gaussian Process Factor Analysis (GPFA) for the same example session after spike sorting into 12 single units. In each of the three panels, each trace is the trial-averaged (\pm one standard deviation) latent activity magnitude, plotted using the same alignment and epoch definitions as in (A). **C.** Latent activity represented in state space for the same example session. Latent activity during each of the four colored epochs are plotted as three-dimensional data points (each 20 ms bin has a magnitude along Factors 1, 2, and 3). Each dot represents the summary of the population activity pattern in a single 20 ms window; thus, a single trial contributes multiple points, even within the same epoch. The trial-averaged trajectory in each epoch is layered above the individual points as a colored trace with black arrows denoting the direction of travel throughout the task timeline. **D.** Amount of covariability across neurons explained by lower-dimensional models compared to the full GPFA model. Each session is represented by a single trace. The majority of sessions have a high amount of shared variance explained by only one to three factors; thus, we retain the first three latent dimensions for each session.

117 In order to justify our comparison of delay period activity against two sets of activity, we first need to
118 demonstrate that the activity patterns produced during the visual and motor epochs are distinct. **Figure**
119 **3A-C** shows the separability of the visual (100 to 200 ms after target onset) and motor (120 to 20 ms
120 before saccade onset) latent activity patterns for three example datasets. By eye, the two subspaces
121 are highly separable for these populations, and this separability was confirmed using linear discriminant
122 analysis classification (**Figure 3D**). Across sessions, the mean classification accuracy was 82.7%
123 ($\pm 11.3\%$), significantly above chance level of 50% (one-tailed t-test). This accuracy was not significantly
124 different when considering multiunit activity (i.e., prior to spike sorting, see **Extended Data Figure 3-1**).
125 Our subsequent analyses required a high level of separability between the visual and motor subspaces.
126 We used a minimum classifier accuracy of 70% as our cutoff criterion, which reduced our yield to 22
127 datasets.

128

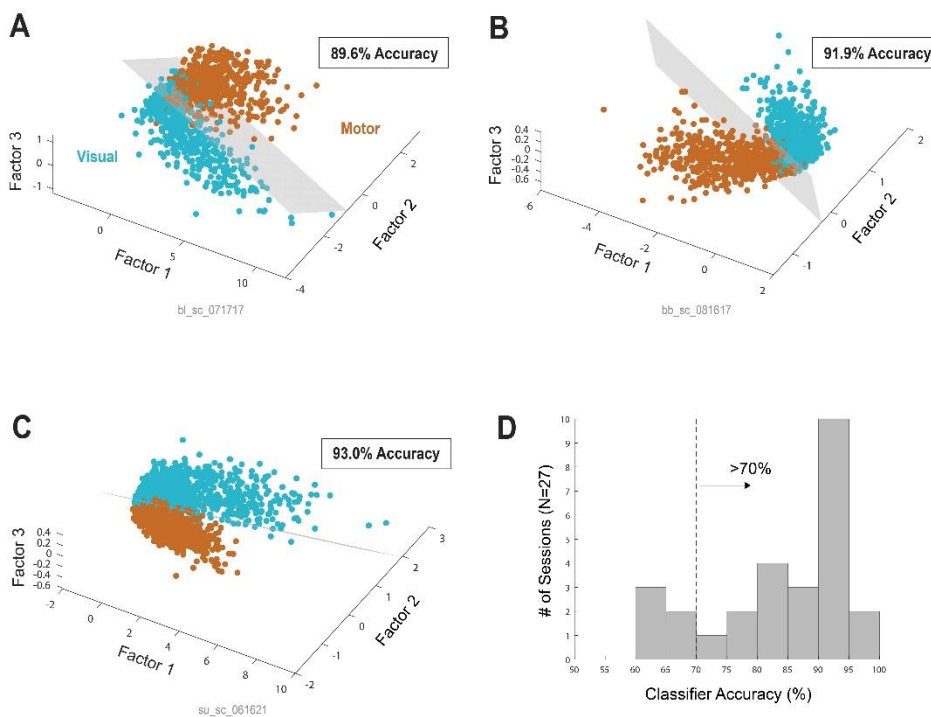


Figure 3. Visual and motor activity are linearly separable in state space for SC neural populations.

A. Subspaces formed by latent activity patterns during the visual (cyan) and motor (orange) epochs for one example session. Time windows used for both epochs and a description of each data point are described in Figure 2. The gray shade indicates the plane of maximal separability as determined by linear discriminant analysis (LDA). The cross-validated classification accuracy of visual and motor points for this example session is also reported. **B-C.** Same as in (A) but for two additional example sessions. **D.** Histogram of linear discriminant classifier cross-validated accuracy in distinguishing visual from motor patterns across all 27 sessions. Only sessions with accuracy values of 70% or better were used in analyses that assume high separation between visual and motor subspaces, leaving 22 sessions for future analyses.

129 **A gradual evolution from visual to motor subspace occurs during sensorimotor transformation**

130 Once we established that visual and motor activity subspaces are separable, we wanted to examine the
131 evolution of latent activity patterns throughout the delay period to determine if there is a consistent
132 trend in the activity pattern from a visual-like representation to a motor-like representation. We utilized a
133 Visuomotor Proximity Index measure (VMPI, see **Methods**) to compute the similarity of the population
134 activity pattern during small windows of time to the visual and motor subspaces (**Figure 4**). As
135 expected, the VMPI is very close to the visual subspace during the visual epoch (cyan shade), to the
136 motor subspace during the movement epoch (orange shade), and in-between during the delay period
137 (purple shade).

138 To evaluate the evolution of population activity in sensorimotor transformation, we plotted the VMPI
139 during the delay period for all sessions before (**Figure 5A**) and after (**Figure 5B**) subtracting the mean of
140 the first ten time bins for each session. These traces were then averaged to compute the session-
141 averaged VMPI shown in **Figure 5C**. This trace reveals a slow, ramp-like progression of activity toward
142 a motor-like representation as time in the delay period progresses. The monotonic trend was small but

143 highly statistically significant ($p < 0.001$, Mann-Kendall test), suggesting that the neural activity pattern
144 slowly and systematically drifts toward a motor-like representation. The evolution of VMPI was highly
145 variable across trials, exhibiting unique but noisy dynamics on individual trials (see two example
146 sessions in [Extended Data Figure 4-1](#)). Therefore, this monotonic trend only became evident when trial-
147 averaging.

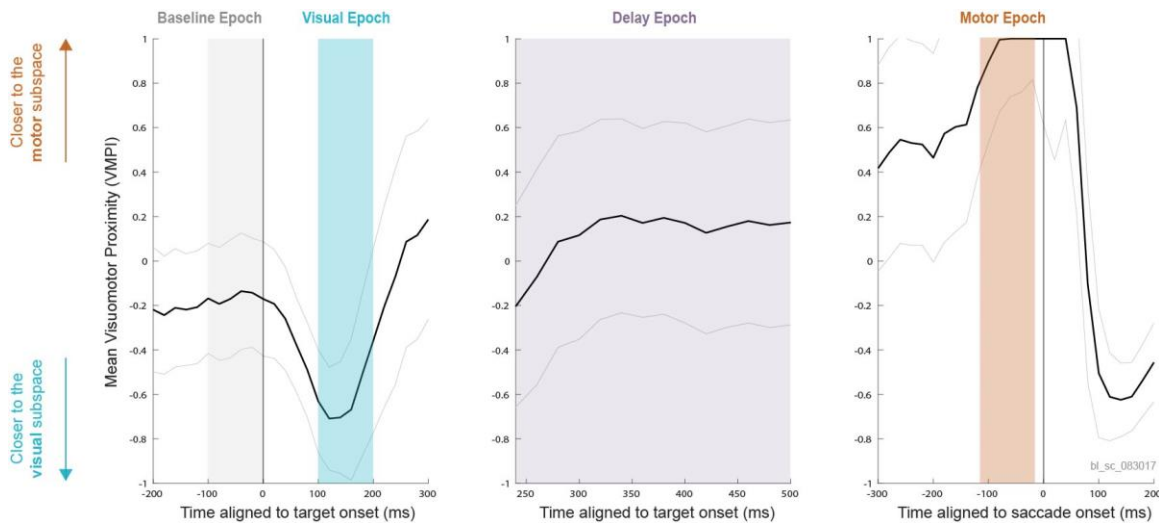


Figure 4. A Visuomotor Proximity Index (VMPI) can characterize the evolution of sensorimotor transformation. Mean (\pm one standard deviation) VMPI values across trials for the same example session as [Figure 2](#). The three panels also obey the same alignment and color scheme. A value closer to +1 indicates similarity of activity to a motor pattern and a value closer to -1 indicates that activity is more similar to the activity pattern produced during the visual epoch. VMPI values are by design limited to the range $[-1, 1]$. The evolution of VMPI across the delay period (purple shaded rectangle) give insights into the representations of SC population activity between the visual and motor epochs.

148 ***Microsaccades transiently revert delay period activity toward visual subspace***

149 Microsaccades are rapid eye movements with kinematics resembling those of larger saccades but
150 characterized by their small magnitude (less than ~ 2 degrees) and are frequently observed during
151 fixational periods, including the delay period studied here (e.g., Hafed et al., 2015; Jagadisan & Gandhi,
152 2016; Peel et al., 2016). Therefore, we questioned if microsaccades that occurred during the delay
153 period produced perturbations in the neural activity pattern that impacted the monotonic trend observed
154 in [Figure 5C](#). Microsaccades were detected offline (see [Methods](#)), and for sessions with a sufficient
155 number of trials with microsaccades ($N=14$), trials in which at least one microsaccade occurred at any
156 point during the delay period were separated from those trials in which no microsaccade was made.

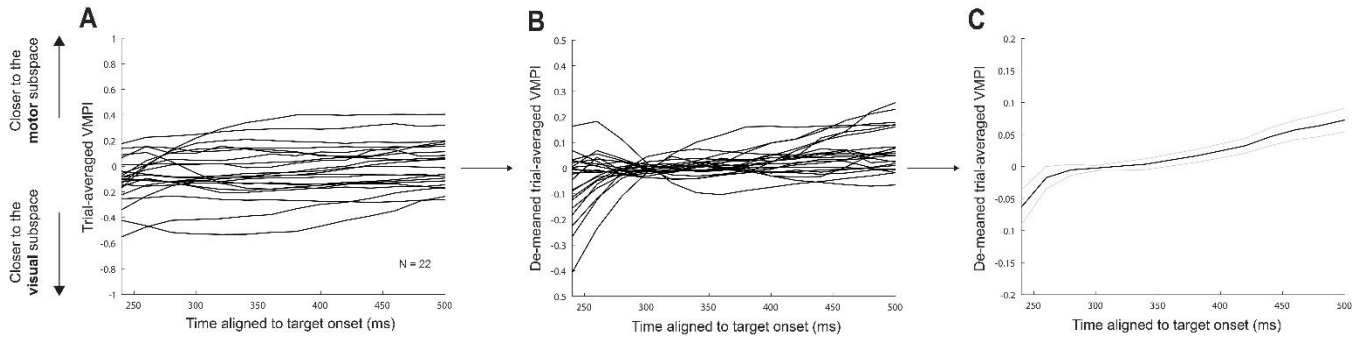


Figure 5. Trial-averaged neural activity slowly drifts from a visual- to a motor-like pattern. **A.** Trial-averaged Visuomotor Proximity Index (VMPI) value across the delay period for the 22 sessions with >70% accurate separability between the visual and motor clusters. Each session is represented as a single trace. **B.** Same as in (A) but with VMPI traces de-meaned for each session separately based on the first ten time bins. This allows us to average the VMPI traces across sessions to generate an across-session representation of the evolution of activity from the visual to motor subspace throughout the delay period, as shown in panel (C). There is a small but highly statistically significant, monotonic trend ($p < 0.001$, Mann-Kendall test) from a more visual- to a more motor-like pattern throughout time in the delay period, indicative of a sensorimotor transformation signature.

157 Interestingly, when we aligned the VMPI value on microsaccade onset (microsaccade trials) or a semi-
158 random delay period time (non-microsaccade trials, see [Methods](#)), we found a large and consistent
159 effect, as illustrated in [Figure 6A](#) for an individual session's data and [Figure 6B](#) as an across session
160 average. Beginning approximately 50 ms after microsaccade onset, the VMPI deviated toward the
161 visual subspace, indicating a pronounced shift toward a visual-like representation that resolved over
162 roughly the next 100 milliseconds. This aligns well with the idea that microsaccades serve to refresh
163 information about the visual stimulus in the SC by jittering the target location on the retina (Khademi et
164 al., 2020). However, at no time in the delay period was there a significant difference between the VMPI
165 values for session-averaged microsaccade and no-microsaccade conditions ([Figure 6C](#)), indicating that
166 the transient microsaccade-induced perturbation of the activity pattern on individual trials did not affect
167 the slow, systematic drift observed on average throughout the delay period.

168 We decided to “zoom out” and see if this visual-like signature following a microsaccade was observable
169 not only at the population level, but at the single neuron level. [Figure 6D](#) shows the trial-averaged firing
170 rates of individual units aligned to microsaccade onset for two example sessions. For the session on
171 the left, the more superficial units – those that typically exhibit a visual burst – clearly increase their
172 firing rates following a microsaccade, consistent with the population-level analysis. This firing rate
173 modulation of superficial units is nowhere near as pronounced for the example session on the right, yet
174 the population-level measure we employed (i.e., VMPI) was able to easily pick up on a change in
175 representation following a microsaccade (compare VMPI in [Figure 6A](#) with same session's individual
176 neuron dynamics in [Figure 6D](#) right panel). We probed this effect further by correlating across all
177 neurons and sessions the post-microsaccade firing rate with the visual burst evoked when a stimulus is
178 presented in the response field ([Figure 6E](#), $R^2 = 0.64$), the motor bursts generated for a saccade to that
179 location ([Figure 6F](#), $R^2 \approx 0$), and each neuron's traditional visuomotor index (see [Methods](#); [Figure 6G](#),
180 $R^2 = 0.34$). The moderately strong relationship between visual activity and activity following a
181 microsaccade confirms that the transient reset toward the visual subspace seen in [Figure 6B](#) in large
182 part arises due to a strong transient increase in the activity of neurons in the population that have a
183 visual burst.

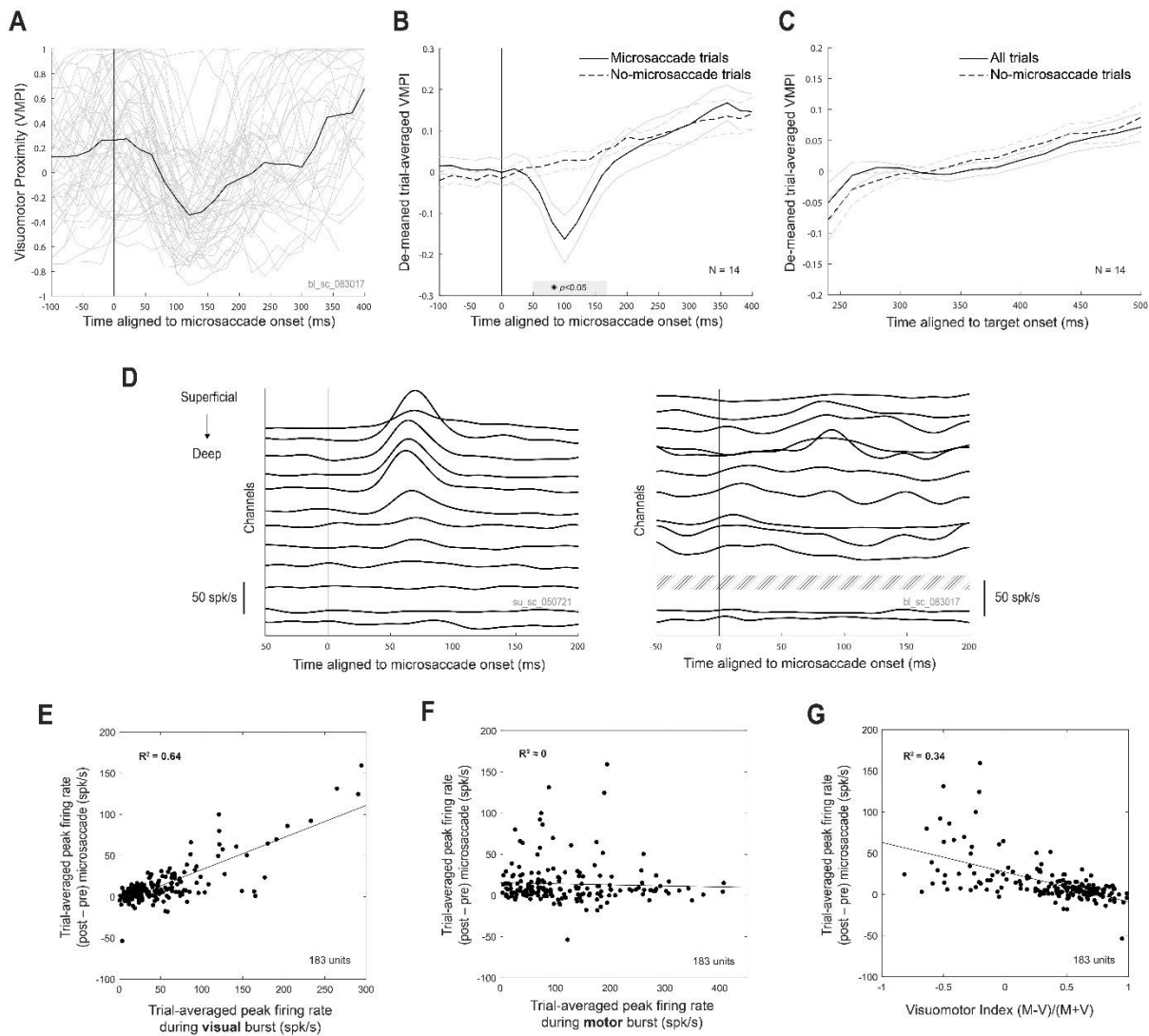


Figure 6. Single-trial population neural activity transiently reverts towards a visual pattern after a microsaccade. A. VMPI values on individual trials (gray) of an example session (same as Figure 2 and Figure 4) in which one or more microsaccades were detected during the delay period, with the median trace shown in black. VMPI values are aligned to microsaccade onset time, regardless of the absolute time in the delay period the microsaccade occurred. On average, the VMPI value dips toward a visual-like pattern ~50 ms following a microsaccade. **B.** Session-averaged, de-measured VMPI values (mean in black \pm one standard error of the mean in gray, as in Figure 5C) aligned to microsaccade onset (solid lines) or pseudo-microsaccade onset on non-microsaccade trials (dashed lines, see Methods). The population activity pattern significantly and transiently deviates from the pattern produced on non-microsaccade trials starting around 50 ms and returns to match the pattern produced on non-microsaccade trials by 170 ms (Wilcoxon rank sum test, $p < 0.05$). **C.** Same setup as in Figure 5C, with de-measured, session-averaged VMPI values throughout the delay period plotted for two groups of trials – all trials (solid lines) and trials in which no microsaccade was detected during the delay period (dashed lines). The two traces never significantly differ from each other (Wilcoxon rank sum test), demonstrating that the presence of microsaccades on some trials does not affect the interpretation of Figure 5C. **D.** Trial-averaged firing rates of individual neurons aligned to microsaccade onset for two example sessions. Each unit is offset vertically based on the channel on which it was recorded (hence, the example session on the right has two units shown on one channel and no units shown on another, as indicated by diagonal shading). For many sessions, the superficial neurons burst following a microsaccade, although in some sessions – such as the example session on the right – it is difficult to appreciate any activity change following a microsaccade when looking at individual neuron firing rates. Still, even for these sessions, there is a population-level transient shift in representation toward a visual-like pattern (see same example session in (A)). **E.** Neurons with a visual response exhibit increased activity levels following a microsaccade. Each point represents a single neuron from a single session. **F-G.** Same setup as in (E) but for the relationship between peak activity around saccade onset (F) or visuomotor index (G) and the peak firing rate following a microsaccade. There is no correlation between the level of motor-related and microsaccade-related firing rates, and there is a lower correlation between the relative visual and motor properties of neurons (using Visuomotor Index, VMI, as a proxy) and microsaccade-related activity than when only the strength of the visual burst is considered (i.e., E).

184 **Sensorimotor transformation process is predictive of reaction time**

185 We show above that on average, SC activity slowly drifts toward a motor-like representation throughout
186 the delay period. This prompted us to ask if the magnitude of this drift on each individual trial was
187 related to the animal's ability to rapidly initiate an eye movement on that trial. We hypothesized that the
188 higher the VMPI at a given time in the delay period (and therefore the larger the drift), the less time it
189 would take the monkey to initiate the saccade after a cue to initiate movement ("go cue") was given on
190 that trial. **Figure 7A** shows the correlation coefficients between the VMPI value at time windows leading
191 up to the animal's go cue and the eventual saccadic reaction time (RT). At the time of the go cue to
192 make an eye movement (time=0 ms, rightmost point of **Figure 7A**), the VMPI value was significantly
193 correlated with the eventual RT, supporting the idea that the amount of drift on an individual trial by the
194 end of the delay period is predictive of the animal's ability to initiate a movement. This relationship held
195 for all time points during the delay period leading up to the go cue (time range of -360 to 0 ms, **Figure**
196 **7A**). No other saccade metrics (i.e., amplitude, peak velocity, endpoint error) were found to be
197 correlated with RT (**Extended Data Figure 7-1, A&B**), nor might we expect them to be (Hafed, 2021).

198 When aligning single-trial VMPI values to the beginning of the delay period (**Extended Data Figure 7-**
199 **1C**), the position of the activity was not correlated to the eventual behavioral output, suggesting that the
200 population representation likely drifts at relatively similar rates across trials. If so, then the drift would be
201 bigger for the longer delay trials, which would be associated with faster reaction times. Indeed, the
202 variable length of the delay period, in the context of our experimental paradigm, seems to account for
203 the variable latency in the behavior (**Extended Data Figure 7-2**).

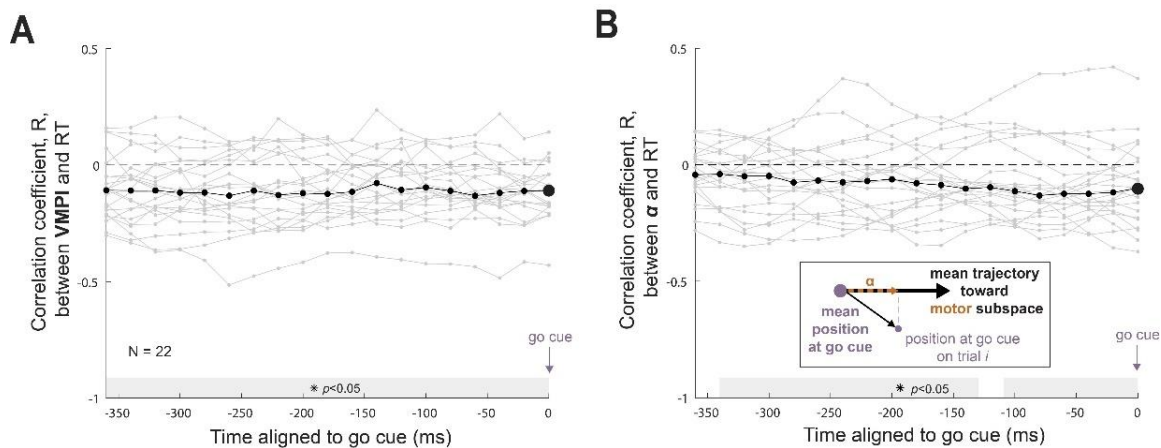


Figure 7. The single-trial state-space position of activity is correlated with that trial's saccadic RT even long before the go cue. **A.** Across-trial correlation coefficient between the VMPI value in a single time bin relative to that trial's go cue time and the eventual saccadic reaction time (RT) on that trial. Each gray trace represents the across-trial correlation coefficients for a single session, with the across-session median trace shown in black. Time bins in which the median correlation coefficients were significantly below zero ($p < 0.05$, one-tailed Wilcoxon signed rank test) are shaded along the x axis in gray. Even long before the go cue, the state space position of activity (as computed via VMPI) is correlated to a behavioral metric. **B.** Same as in (A) but for correlations between a single trial's projection value α and that trial's saccadic RT. Each projection value α represents the distance traveled along the trial-averaged neural trajectory toward the motor subspace by a certain time relative to the go cue on a given single trial i , with the method for finding α shown in the inset. Methodology was previously used in Afshar et al., 2011, and applied here to SC neural populations. This different method of computing state-space position of activity reveals a similar correlation to saccadic RTs, up to 340 ms before the go cue on average.¹

204 This finding conforms well to an existing theory of arm movement generation – the initial condition
205 hypothesis (Afshar et al., 2011; Churchland et al., 2006) – in which the population activity pattern at the
206 animal's go cue informs the latency of the reach initiation on that trial. Critically, however, the brain

207 areas relevant to reach initiation (e.g., primary motor cortex and dorsal premotor cortex) do not have
208 significant responses to visual stimuli. Because of the strong visual bursts exhibited by SC neurons, we
209 wanted to ensure that the relationship between population activity pattern and latency of saccade
210 initiation remains even when disregarding the visual-likeness of the pattern during the delay period.
211 Therefore, we decided to employ an additional methodology (mirroring that of Afshar et al., 2011) that
212 only considers the position and trajectory of activity patterns relative to the patterns underlying *motor*
213 output rather than relative to activity during both the visual *and* motor epochs (as is the case with the
214 VMPI metric). In short, two vectors are created – one that extends from the mean activity position at the
215 time of the go cue to some short time later (100 ms) and another that extends to the actual position at
216 the time of the go cue (or before) on an individual trial (shown in Figure 7B inset). The projection value
217 α obtained by projecting the latter vector onto the former gives you a magnitude that can be thought of
218 as distance traveled toward the motor subspace by a certain time in the delay period.

219 When applying these methods to SC population activity, we found that the correlation values closely
220 matched both those applied previously to premotor cortex activity and those obtained through our VMPI
221 – RT correlation analysis. Across many populations, the median correlation between projection value at
222 the go cue and RT across trials was small but significant (Figure 7B, data points at t=0 ms), similar to
223 the results of the VMPI – RT correlation analysis (i.e., Figure 7A). Also comparable was the significant
224 correlation between projection value α and eventual RT even long before the go cue (Figure 7B, data
225 points leading up to t=0 ms). Therefore, this relationship between the population-level activity pattern
226 and movement initiation latency holds even when only considering the motor-likeness of the pattern.
227

228 DISCUSSION

229 In this study, we sought to understand whether population activity in the SC systematically transitions
230 from a visual-like pattern to a motor-like pattern throughout the delay period and found that on average,
231 the activity pattern (as measured by the VMPI value) did indeed slowly drift from a visual-like to a
232 motor-like representation. Notably, following a microsaccade, the activity pattern was characterized by
233 a transient reset to a visual-like representation (Figure 8A). In addition, the amount of drift exhibited by
234 the population at times leading up to the animal's go cue on individual trials was predictive of the
235 latency at which a saccade could be initiated on that trial. On the other hand, neither the starting
236 representation nor the amount of drift aligned to the beginning of the delay period were related to the
237 eventual saccade latency. Together, these findings lead us to conclude that activity drifts at a relatively
238 consistent rate across trials and sets the animal up for a shorter or longer latency saccade based on
239 the amount of time the activity has had to drift on a given trial (Figure 8B). This study therefore provides
240 new insights into the neural dynamics expressed within the SC during the delay period of a widely used
241 behavioral task.

242 Our population-level results disclosed a gradual evolution from a sensory-like to motor-like
243 representation that is consistent with the interpretations provided from previous studies on sensorimotor
244 transformation in the SC (e.g., Lee and Groh, 2012; Sajad et al., 2020; Sadeh et al. 2020). If the SC is
245 indeed involved in sensorimotor transformation, then we could have expected to observe a few possible
246 alternate dynamics in the visual-like or motor-like representations throughout the delay period. First,
247 activity patterns could oscillate between the visual and motor subspaces, balancing two needs –
248 retaining information about the sensory stimulus and preparing for a movement. This is akin to the idea
249 of maintaining simultaneous representation of multiple auditory stimuli (Caruso et al., 2018a). Second,
250 activity patterns could lack a consistent trend toward either subspace across the delay period,
251 potentially encoding features independent of sensory information or movement preparation (Kaufman et
252 al., 2015). Third, activity patterns could exhibit a discrete switch, or step, from one representation to the
253 other (Latimer et al., 2015). Instead, the slow evolution we saw in SC population activity patterns

254 toward a motor-like pattern is evidence of a smooth and slow drift in representation between the times
255 of sensation and action. Furthermore, recognize that the subspaces labeled as sensory and motor are
256 merely a reduced dimensional representation of the population activity. Importantly, they are agnostic to
257 the reference frame represented by the neural activity. Finally, we note that the gradual transition was
258 only observed when averaging across trials. Despite the many benefits of dimensionality reduction,
259 neural activity on single trials is still inherently noisy, and thus the lack of quantifiable trend on individual
260 trials does not decrease our confidence that the across-trial sensorimotor transformation trend is
261 meaningful.

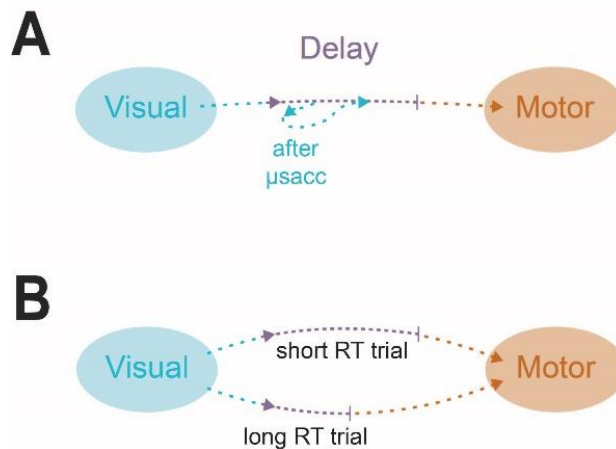


Figure 8. Schematics representing the evolution of SC population activity throughout the course of a standard sensorimotor task. A. Characteristic time course of population activity during the delay period. On average, population activity slowly becomes less visual-like (visual subspace shown as a cyan ellipse) and more motor-like (orange ellipse) throughout time in the delay period (purple dotted line). Following a microsaccade, when it occurs, population activity transiently and strongly deviates its trajectory toward the visual subspace (cyan dotted line) before returning to the characteristic route toward the motor subspace. Vertical purple line denotes VMPI at go cue. **B.** Depiction of the population activity trajectories on microsaccade-absent trials with short (top) and long (bottom) saccadic reaction times. Activity during the delay period likely evolves at a comparable rate across trials, at least under the experimental conditions we used. However, the activity can continue its slow drift toward the motor subspace for a longer time on trials with longer delay period lengths (top) than on those with shorter delay period lengths (bottom), thereby only necessitating a limited distance to travel to the motor subspace once the cue to initiate the behavior is given (vertical purple line).

262 In one study, subpopulations of cortical oculomotor neurons categorized based on their relative firing
263 rates during the visual and motor epochs were shown to exhibit unique temporal dynamics of this
264 reference frame transformation, in contrast to the smooth and gradual transition observed when treating
265 all neurons as a single population (Sajad et al., 2016). The VMPI measure we use implicitly takes into
266 account the activities of all neural subtypes (i.e., visual, visuomotor, and motor) and produces one
267 concise value, although the neurons recorded in this study were by and large visuomotor neurons.
268 Research that specifically teases apart the individual contributions of neural subtypes to the time
269 course of sensorimotor transformation may be required for a more complete understanding of the SC
270 correlate of this behavioral phenomenon. Also not considered within this study are cognitive factors
271 such as reward anticipation, arousal, and attention – factors which may in fact be multiplexed with
272 encoded visual and motor signals present in the SC. Thus, the exact relationship of delay period SC
273 activity patterns to phenomena other than visual processing and movement initiation is ripe for future
274 investigations.
275

276 ***Does SC delay activity resemble a preparatory signal?***

277 The results shown in [Figure 7A and 7B](#) suggest that a relationship between the activity pattern and the
278 reaction time (RT) of the eventual saccade is present long before permission is granted to initiate the
279 movement. In other words, if the pattern of SC population activity drifts close to the motor subspace
280 (i.e., has a high VMPI value) during the delay period of a given trial, the activity will take little time to
281 evolve into a fully motor-like pattern after the go cue, resulting in a low-latency saccade. In the context
282 of our task design, SC delay period activity seems to drift in representation at a relatively equal rate
283 across trials ([Extended Data Figure 7-1C](#)). It is on trials with longer delays that the population activity
284 has extra time to evolve, and therefore continues to drift toward a motor-like representation
285 (equivalently, an increasing VMPI) proportional to the delay period length, resulting in proportionally fast
286 reaction times ([Extended Data Figure 7-2](#)).

287 The observation that the rate of drift is unmodulated from one trial to another could be reflective of the
288 animal's internal model of the expected delay period length distribution. To extrapolate, if the delay
289 period length was known by the animal to instead be constant, the activity pattern may still drift at
290 slightly different rates from trial to trial, which we posit would constitute preparatory activity and serve
291 as a mechanism for movement initiation. Regardless, the schematic shown in [Figure 8](#) is inclusive of
292 both schemas.

293 The consistent rate of sensorimotor evolution from trial to trial leads us to consider whether this drift
294 might act as a self-timing mechanism, indicative of perceived time elapsed in the delay period. Suppose
295 the monkey employs a strategy in which he begins to expect a delay period length somewhere in
296 between the shortest and longest delays previously experienced (as observed in human studies;
297 Jazayeri & Shadlen, 2010). If he consistently plans to initiate an eye movement after this expected
298 delay period length, he may receive the benefit of more frequently successful trials (and consequently,
299 more frequent and more rapid rewards) since he has optimized the timing of his saccade to match his
300 expectation. Neurons in the macaque thalamus (Tanaka, 2007) and lateral intraparietal cortex (Leon
301 and Shadlen, 2003) have been shown to encode perceived time intervals. Perhaps the drifting
302 representation we observe in SC populations is another signature of task timing. Further experiments
303 might explore this concept and its validity.

304 Although we consider SC activity during the delay period to be preparatory in the sense that it is related
305 to the enhancement or hindrance of rapid saccade initiation following the go cue, it does not have
306 "motor potential." In the smooth pursuit system of the FEF, neural activity was found to have motor
307 potential, with partially overlapping subpopulations contributing to both the preparation and execution of
308 movement (Darlington and Lisberger, 2020). However, this does not seem to be the case for the SC, at
309 least in the context of saccades. Previously, we have demonstrated that inhibition of the omnipause
310 neurons during the delay period, which allows SC activity to travel to saccade-generating brainstem
311 structures, is not sufficient to evoke a saccade (Gandhi and Bonadonna, 2005; Jagadisan and Gandhi,
312 2017). In addition, the lack of a burst and only a baseline-level "temporal stability" – that is, the
313 consistency in the population activity pattern from one time point to another – enhance the argument
314 against delay activity having motor potential (Jagadisan and Gandhi, 2022). We have also observed
315 that it is typically the neurons with strong visual bursts rather than strong motor bursts that have
316 sustained activity during the delay period (Massot et al., 2019). Therefore, it stands to reason that
317 preparatory signals are likely encoded in the SC in dimensions orthogonal to those during movement
318 (e.g., orthogonal potent-null subspaces; Kaufman et al., 2014).

319

320 ***The relationship between microsaccades and SC population activity patterns***

321 Microsaccades produced during fixation serve to refresh the visual stimulus on the retina in order to
322 combat a fading perception over time (Martinez-Conde et al., 2004). The neural circuit in SC
323 suppresses vision during microsaccades (Hafed and Krauzlis, 2010), as it does during large amplitude
324 saccades (Robinson and Wurtz, 1976). Following the movement, the nervous system responds to its
325 visual environment by evoking activity in visually responsive neurons, although extra-retinal sources
326 likely contribute as well. Indeed, we observed that microsaccades produced during the delay period
327 consistently perturbed the sensation to action transition by transiently deviating SC population activity
328 toward the visual subspace. The effect was strongest in the subset of neurons with a robust visual
329 response. This modulation began roughly 50 ms after microsaccade onset and peaked another 50 ms
330 later before rapidly meeting back up with the population activity patterns observed in non-microsaccade
331 trials. Thus, the resurgence of visual activity likely reflects visual reafference following the movement
332 (also see Khademi et al., 2020).

333 It is valuable to consider the various ways in which microsaccades generated during the delay period
334 could have impacted the oculomotor system. For instance, the movement-related activity associated
335 with microsaccade generation could have accelerated the overall SC output toward the motor
336 subspace, resulting in reduced saccade latency – perhaps even triggering it prematurely before the go
337 cue – and altered endpoint accuracy (Buonocore et al., 2021). Instead, we observed a rapid rebound
338 and return of the system (VMPI trace, [Figure 6B](#)) to its original trajectory following a microsaccade. We
339 interpret this reset to suggest that the gradual transition from a sensory to motor representation may be
340 a network feature that is resistant to the effects of transient disruptions. As a whole, these observations
341 lead us to conclude that microsaccades are a potential mechanism for engaging the network to produce
342 a visual-like signal very similar to that elicited in response to the initial target appearance, but one that
343 is compensated for quickly and robustly.

344

345 ***Low-dimensional geometry of SC population activity and its skeletomotor counterparts***

346 One of our objectives was to extend to the oculomotor system the dynamical systems perspective of
347 motor control that has been studied extensively in the skeletomotor system (Gallego et al., 2017;
348 Shenoy et al., 2013). Studies of arm reaching that use this framework have given rise to multiple
349 hypotheses for mechanisms of movement initiation. One such schema is the “optimal subspace
350 hypothesis” (Churchland et al., 2006), which propounds that there is an optimal set of population
351 activity patterns that allow for the generation of a goal-directed movement. The initial condition
352 hypothesis (Afshar et al., 2011) builds on this framework by postulating that trials in which patterns that
353 have traveled closer to the motor subspace by the time of the animal’s go cue will have a faster
354 reaction time (RT) than those in which the underlying neural activity has not traveled as far along the
355 mean neural trajectory.

356 It might make sense for the oculomotor system to operate in a somewhat different manner than the
357 skeletomotor system given the additional element – visual information – encoded within the SC and
358 other oculomotor areas. However, even when considering this additional set of patterns exhibited by
359 SC populations, we found that on trials in which population activity more closely resembles a motor-like
360 pattern, the saccadic RT is significantly shorter ([Figure 7A](#)).

361 To establish a more direct comparison between SC activity and activity in its skeletomotor analogs, we
362 also applied the methods of Afshar et al., 2011, to SC population activity during the delayed saccade
363 task and found a comparable, significant correlation between the position of delay period activity and
364 the saccadic RT ([Figure 7B](#)). Although the exact methodologies applied in [Figure 7A and 7B](#) are
365 distinct, they address similar questions – primarily, is the similarity of neural activity during the delay

366 period to motor activity related to the speed at which the movement can be initiated (i.e., eye movement
367 or reaching movement RT). The findings reported in this study support the idea that the initial condition
368 hypothesis is also valid for the oculomotor system.

369 The optimal number of dimensions needed to explain the across-trial shared variance of our acutely
370 recorded neural populations was much lower than that described in studies using neural activity
371 recorded in primary motor cortex (M1) or dorsal premotor cortex (PMd), for example (Churchland et al.,
372 2010; Churchland and Shenoy, 2007). We conjecture that this is at least partially due to the
373 homogeneity of each recorded population. As SC neurons are traditionally recorded along a
374 dorsoventral axis, the topography of the SC yields populations in which each neuron has a similar
375 response field, chiefly varying across electrode depth in the strength of their visual and motor bursts
376 (Massot et al., 2019). Cortical areas like M1 and PMd yield much more heterogenous populations with
377 respect to the spatial locations preferentially encoded by each neuron, and the dynamics underlying
378 behavior are typically studied after grouping trials with multiple reach directions. However, since our
379 recorded SC populations vary not in their preferred spatial location but rather in their visual and motor
380 signal strengths, we limited our analyses to a single saccade direction so that in reducing the
381 dimensionality of the data, the variability between visual and motor patterns would be brought to the
382 forefront.

383

384 **MATERIALS AND METHODS**

385 ***Subjects and surgical approach***

386 Three adult male rhesus monkeys (*Macaca mulatta*; monkeys BL, BB, and SU) were used for this
387 study. The experimental protocol was approved by the University of Pittsburgh Institutional Animal Care
388 and Use Committee. Each animal underwent a sterile surgery under general anesthesia to implant a
389 cylindrical recording chamber (Narishige) positioned above a craniotomy that allows access to the SC.
390 A Teflon-coated, stainless-steel wire was also implanted on one eye in some animals. Surgical
391 methods are described in more detail in Jagadisan & Gandhi, 2016.

392

393 ***Visual stimuli and behavioral paradigm***

394 Stimulus presentation and the animal's behavior were under real-time control with a LabVIEW-based
395 controller interface (Bryant and Gandhi, 2005). All stimuli were white squares, 4x4 pixels subtending
396 approximately 0.5°, displayed against a dark grey background on a LED-backlit flat screen monitor. Eye
397 position was recorded using the scleral search coil technique (CNC Engineering) or using an EyeLink
398 1000 eye tracker (SR Research), both sampled at 1 kHz.

399 Each monkey was trained to sit head-restrained in a primate chair and perform a standard delayed
400 saccade task in a dimly lit room. To complete a successful trial of this task, the monkey fixated on a
401 visual stimulus located in the center of the screen and maintained fixation while a visual target was
402 presented in the animal's periphery. After a variable delay period (600-1200 ms for monkeys BL and
403 BB, and 700-1500 ms for monkey SU, weighted to maintain a flat anticipation function), the fixation
404 point was extinguished, serving as the animal's "go cue" to make a saccadic eye movement to the
405 target. The animal had to make a saccade to the peripheral target within 460-800 ms and was required
406 to maintain fixation on it for 300 ms to receive a liquid reward. The monkeys performed this task with
407 high accuracy before recording sessions began. Thus, we limited our analyses to rewarded trials only.

408

409

410 ***Electrophysiology and data pre-processing***

411 On each recording session, a 16- or 24-channel linear microelectrode array (Plexon or AlphaOmega)
412 was inserted orthogonal to the SC surface along the dorsoventral axis. Neurons recorded using this
413 approach had similar preferred saccade vectors as determined by microstimulation (Massot et al.,
414 2019). Care was taken to position the electrode in a way that maximized the yield of neurons exhibiting
415 both visual and motor bursts, and thereby tended to be positioned in the deeper SC layers.

416 On each given trial, the target presented in the animal's periphery could be located near the center of
417 the response field of the recorded neurons (as determined by microstimulation) or in the diametrically
418 opposite position with a 2:1 ratio of occurrence. Only correct trials in which the target was presented in
419 the recorded neurons' response field were included in analyses, and all analyses were performed
420 separately for each neural population. Trials were further limited to only those with saccadic reaction
421 times of greater than 100 ms to remove potential "cheat" trials. Unless otherwise specified, all analyses
422 were performed using MATLAB 2019a (MathWorks) with custom code.

423 Spike times on each channel were first obtained offline using a voltage thresholding method. Each
424 channel's spiking activity was then manually sorted into single units before continuing with analyses
425 (using MKsort, a spike-sorting user interface, Ripple Neuro), and the low-dimensional representations
426 of population activity are quite similar (see [Extended Data Figure 3-1](#)). This is in line with previous work
427 demonstrating that spike sorting has a negligible effect on the message of studies that focus on low-
428 dimensional dynamics of population neural activity (Trautmann et al., 2019). Therefore, throughout the
429 text we present results from spike-sorted neural activity but think of units (neurons) and multiunits
430 (channels) as interchangeable. A total of 27 sessions were obtained and included in this study.

431

432 ***Dimensionality reduction***

433 In order to analyze the spiking patterns across the entire population, we utilized a dimensionality
434 reduction method called Gaussian-process factor analysis, or GPFA (Yu et al., 2009). In short, this
435 method converts spiking activity from a neural population into a lower-dimensional continuous "neural
436 trajectory," where each dimension represents a weighted linear combination of neurons.

437 To perform GPFA, we used DataHigh (Cowley et al., 2013), a publicly available MATLAB code package
438 for visualizing and reducing dimensionality of high-dimensional neural data. For a given session of
439 laminar electrode data, all channels' spike times were first converted into spike trains aligned on target
440 onset. Spike counts were grouped into non-overlapping bins of 20 ms width. Each observation includes
441 data from one trial of the delayed saccade task beginning 200 ms before target onset and continuing
442 through 200 ms post-saccade. This matrix is of size N channels x T time bins for each trial, with the
443 latter dimension having a variable length. The GPFA algorithm returns a set of latent activity values
444 summarizing the activity pattern across the population for each trial (matrix of L latent dimensions x T
445 time bins for each trial). A cross-validation procedure was performed to determine the optimal number
446 of reduced dimensions. The optimal dimensionality for each found via cross-validation was typically low
447 (one to three). A final dimensionality of three was chosen for the sake of consistency across sessions
448 and for ease of visualization in a 3D state space, as described next.

449

450 ***Defining subspaces and computing proximity***

451 The term "subspace" does not have a widely agreed-upon definition; some groups call each factor
452 returned by dimensionality reduction a subspace in which latent neural activity could be varying (e.g.,
453 Kaufman et al., 2014) while others define new axes and focus on the variable activity along that
454 dimension (e.g., Kobak et al., 2016; Libby & Buschman, 2021) or project activity onto an axis, plane, or

455 hyperplane contained within a higher-dimensional space (e.g., Aoi et al., 2020; Semedo et al., 2019).
456 Here, we more loosely define a subspace as a distinct region in a low-dimensional state space
457 occupied by neural activity during a specified condition (as in Churchland et al., 2006). The two main
458 conditions here are “visual,” or 100 to 200 ms after target onset (around the time of the putative visual
459 burst) and “motor,” or 120 ms to 20 ms before saccade onset (around the rising phase of the putative
460 motor burst, and not including activity from after the latest time it is likely related to saccade initiation;
461 see (Gandhi & Keller, 1999; Jagadisan & Gandhi, 2017; Miyashita & Hikosaka, 1996; Smalianchuk et
462 al., 2018). A baseline condition was also defined, and this includes activity from 100 ms before target
463 onset up to the time of target onset. These comprise the visual, motor and baseline subspaces,
464 respectively.

465 For [Figure 3](#), linear discriminant analysis (LDA) was performed to find the 2D projection that best
466 separates visual and motor subspaces from each other. For each session, a two-class (“visual” and
467 “motor” categories) linear discriminant classifier was trained and tested using a 10-fold cross-validation
468 procedure. Only sessions for which the population activity was sufficiently separable between the visual
469 and motor epochs (>70% classification accuracy rounded to the nearest integer, see [Figure 3D](#)) were
470 further analyzed, leaving 22 sessions that met this criterion.

471 Given that the visual and motor activity (cyan and orange points, respectively) form distinct subspaces,
472 we can use these as reference distributions against which to compare activity from time points
473 throughout the course of each trial. We utilized a measure known as the proximity index, introduced by
474 Dekleva et al., 2018. In short, the proximity index is a probabilistic measure that indicates the relative
475 likelihood that a point of activity is closer in state space to a particular cluster than any other
476 comparison cluster. For a single time bin of latent activity S , its proximity to the visual or motor cluster
477 (VPI or MPI, respectively) is given by:

$$478 \quad \text{Proximity}(S, \{C_i\}) = \frac{P(D_M(S, \{C_i\})|i)}{\sum_{j=1}^3 P(D_M(S, \{C_i\})|j)}$$

479 where $\{C_i\}$ is the cluster of latent activity points during one of three reference conditions, denoted by i
480 and j (here: visual, motor, or baseline) and $D_M(S, \{C_i\})$ is the Mahalanobis distance between the point S
481 and cluster $\{C_i\}$. The VPI is formed when i =visual activity (and j =motor and baseline) and likewise, the
482 MPI is formed when i =motor activity. The VPI and MPI are normalized to the range $[0, 1]$.

483 Since visual and motor proximity indices must be computed separately and result in two yoked values,
484 we defined a visuomotor proximity index (VMPI) that can range from -1 to $+1$ and gives the relative
485 proximity value of a point of activity to either the visual (-1) or motor ($+1$) subspace:

$$486 \quad \text{VMPI} = \frac{\text{MPI} - \text{VPI}}{\text{MPI} + \text{VPI}}$$

487 For [Figure 4](#), the VMPI was computed for all non-overlapping 20 ms bins of latent activity throughout
488 the time course of each trial. Activity from the baseline condition was treated as a third cluster to allow
489 for the possibility of delay period activity existing in a completely different subspace than either the
490 visual or motor subspaces, although proximities to this cluster are unimportant and hence not shown. It
491 is also important to note that the absolute VMPI value ranges are inconsistent across populations (e.g.,
492 [Figure 5A](#)), but this does not matter for our study. Only the dynamics in the VMPI trace over the course
493 of the delay period are of interest; thus, in [Figure 5B-C](#) and [Figure 6B-C](#) each population’s VMPI trace
494 was mean-subtracted to allow for a better comparison of sensorimotor transformation across
495 populations.
496

497 ***Detecting microsaccades and aligning proximity to microsaccade onset***

498 All microsaccades that occurred during the delay period of each trial were detected offline. A 20 ms
499 moving average of the eye velocity was taken, and a speed threshold of 5 to 15 deg/s was applied
500 depending on noise level in the eye position signal. Saccades greater than 2 degrees in amplitude were
501 rejected. Individual trials were manually evaluated to confirm correct automatic detection. Sessions
502 were included in the following analysis if there were at least 20 trials in both the “one or more
503 microsaccades” and “no microsaccades” conditions. One monkey (BB) did not consistently produce
504 microsaccades during the delay period, as we have reported previously (Jagadisan and Gandhi, 2016).
505 Hence, we could only include data from one session for this monkey using the above criteria. Monkeys
506 BL and SU had five and eight sessions that met the above criteria, respectively, for a total of 14
507 sessions included in this set of analyses.

508 To determine the effect of microsaccades on the population activity pattern, we aligned the VMPI to
509 microsaccade onset for trials in which at least one microsaccade was detected during the delay period.
510 As a control analysis, we also aligned the VMPI to a pseudo microsaccade onset time for trials in which
511 there was no microsaccade detected. For each trial, this alignment time was created by selecting a
512 random time from the distribution of microsaccade onset times in trials with a microsaccade ([Figure 6A-](#)
513 [B](#)). As in [Figure 5](#), each population’s trace was mean-subtracted to better compare trends across
514 sessions.

516 ***Computing relationship between population activity patterns and behavioral metrics***

517 To examine whether the position in state space is related to the end behavior (i.e., saccade), we
518 computed the correlation between the VMPI value at the animal’s go cue and the eventual saccadic
519 reaction time (RT) on that trial. We also asked if the position of the activity even leading up to the go
520 cue was correlated with the end behavior. For this analysis, we worked backwards to compute the
521 correlation coefficient of every 20 ms bin of activity with the saccadic reaction times on their respective
522 trials. Values were tested for significance using a Wilcoxon rank sum test.

523 We also employed a similar approach developed by Afshar et al., 2011, that only utilizes information
524 about the putative motor subspace rather than the visual subspace. In this framework, one can ask
525 whether the distance traveled along the mean neural trajectory at the end of the delay period
526 (equivalently, at the time of the animal’s go cue), correlates with the saccadic RT on that trial. These
527 methods have been described previously and were followed as closely as possible. In short, on a single
528 trial, a vector of spike counts across the population starting at the time of go cue and going forward
529 some short time in the future ($dt=100$ ms) is created. This vector is projected onto the vector created by
530 mean values across all trials to obtain a projection value α ([see Figure 7B inset](#)). A correlation
531 coefficient value between saccadic reaction time and this projection value was obtained for each
532 session. To compute the correlation between activity prior to the go cue and the end behavior, we used
533 the same value of dt (100 ms) but worked backwards to compute the median correlation coefficient of
534 every 20 ms bin of activity with the RTs on their respective trials, as in the VMPI – RT correlation
535 analysis. Of note, unlike all other results presented in this paper, this analysis was performed on spike-
536 sorted but not dimensionality-reduced neural activity for a more direct comparison of findings across
537 brain areas.

538

539 **ACKNOWLEDGEMENTS**

540 N.J.G. was supported by NIH R01 EY024831 and R01 EY022854. M.R.H. was supported by the ARCS
541 Foundation, GAANN Fellowship Program (P200A150050), and Behavioral Brain Research Training

542 Program (NIH T32 GM081760). The authors would like to thank Dr. Benjamin Cowley for thoughtful
543 discussions and Dr. Brian Dekleva for providing a template code for the proximity analysis.

544 **REFERENCES**

545

546 Afshar, A., Santhanam, G., Yu, B.M., Ryu, S.I., Sahani, M., Shenoy, K. v., 2011. Single-trial neural
547 correlates of arm movement preparation. *Neuron* 71, 555–564.
548 <https://doi.org/10.1016/J.NEURON.2011.05.047>

549 Aoi, M.C., Mante, V., Pillow, J.W., 2020. Prefrontal cortex exhibits multidimensional dynamic encoding
550 during decision-making. *Nature Neuroscience* 23, 1410–1420. [https://doi.org/10.1038/s41593-020-](https://doi.org/10.1038/s41593-020-0696-5)
551 0696-5

552 Basso, M.A., May, P.J., 2017. Circuits for Action and Cognition: A View from the Superior Colliculus.
553 *Annual Review of Vision Science* 3, 197. [https://doi.org/10.1146/ANNUREV-VISION-102016-](https://doi.org/10.1146/ANNUREV-VISION-102016-061234)
554 061234

555 Bharmauria, V., Sajad, A., Yan, X., Wang, H., Crawford, J.D., 2021. Spatiotemporal Coding in the
556 Macaque Supplementary Eye Fields: Landmark Influence in the Target-to-Gaze Transformation.
557 *eNeuro* 8, 1–23. <https://doi.org/10.1523/ENEURO.0446-20.2020>

558 Bryant, C.L., Gandhi, N.J., 2005. Real-time data acquisition and control system for the measurement of
559 motor and neural data. *Journal of Neuroscience Methods* 142, 193.
560 <https://doi.org/10.1016/J.JNEUMETH.2004.08.019>

561 Buneo, C.A., Jarvis, M.R., Batista, A.P., Andersen, R.A., 2002. Direct visuomotor transformations for
562 reaching. *Nature* 416, 632–636. <https://doi.org/10.1038/416632A>

563 Buonocore, A., Tian, X., Khademi, F., Hafed, Z.M., 2021. Instantaneous movement-unrelated midbrain
564 activity modifies ongoing eye movements. *Elife* 10. <https://doi.org/10.7554/ELIFE.64150>

565 Caruso, V.C., Mohl, J.T., Glynn, C., Lee, J., Willett, S.M., Zaman, A., Ebihara, A.F., Estrada, R.,
566 Freiwald, W.A., Tokdar, S.T., Groh, J.M., 2018a. Single neurons may encode simultaneous stimuli
567 by switching between activity patterns. *Nature Communications* 9, 2715.
568 <https://doi.org/10.1038/s41467-018-05121-8>

569 Caruso, V.C., Pages, D.S., Sommer, M.A., Groh, J.M., 2018b. Beyond the labeled line: Variation in
570 visual reference frames from intraparietal cortex to frontal eye fields and the superior colliculus.
571 *Journal of Neurophysiology* 119, 1411–1421.
572 <https://doi.org/10.1152/JN.00584.2017/ASSET/IMAGES/LARGE/Z9K0031845230005.JPEG>

573 Churchland, M.M., Shenoy, K. v., 2007. Temporal complexity and heterogeneity of single-neuron
574 activity in premotor and motor cortex. *Journal of Neurophysiology* 97, 4235–4257.
575 <https://doi.org/10.1152/JN.00095.2007/ASSET/IMAGES/LARGE/Z9K0050782070017.JPEG>

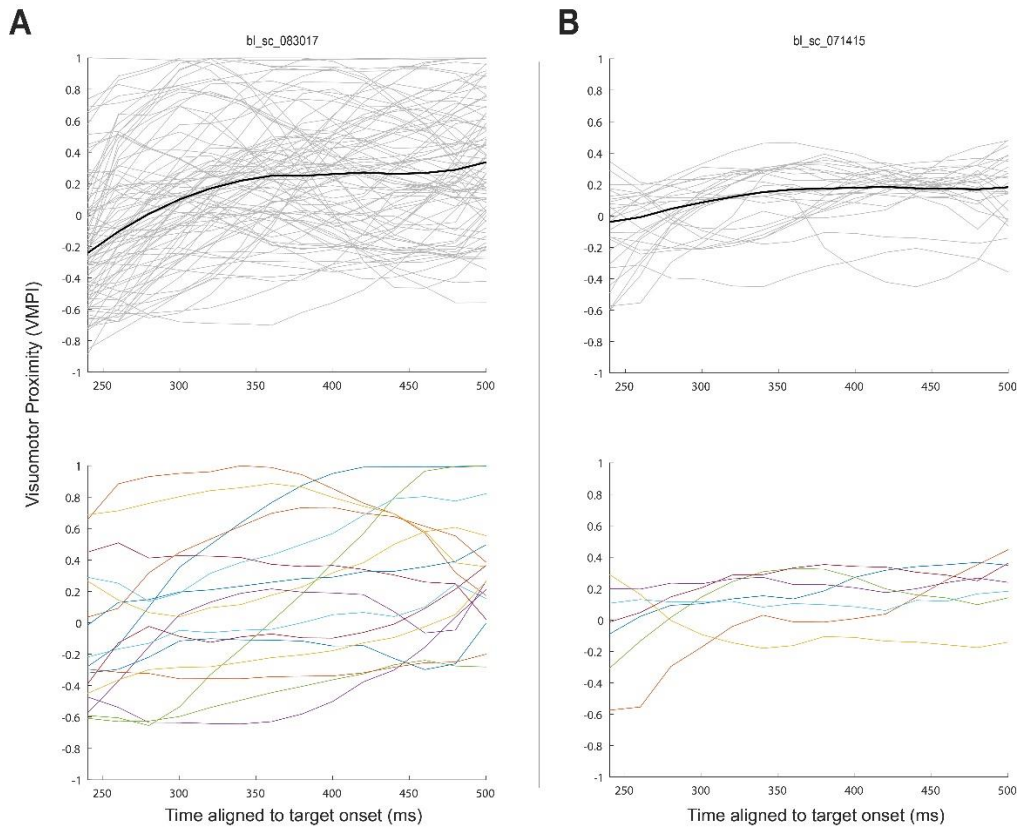
576 Churchland, M.M., Yu, B.M., Cunningham, J.P., Sugrue, L.P., Cohen, M.R., Corrado, G.S., Newsome,
577 W.T., Clark, A.M., Hosseini, P., Scott, B.B., Bradley, D.C., Smith, M.A., Kohn, A., Movshon, A.,
578 Armstrong, K.M., Moore, T., Chang, S.W., Snyder, L.H., Lisberger, S.G., Priebe, N.J., Finn, I.M.,
579 Ferster, D., Ryu, S.I., Santhanam, G., Sahani, M., Shenoy, K. v., 2010. Stimulus onset quenches
580 neural variability: a widespread cortical phenomenon. *Nature Neuroscience* 13, 369–380.
581 <https://doi.org/10.1038/nn.2501>

582 Churchland, M.M., Yu, B.M., Ryu, S.I., Santhanam, G., Shenoy, K. v., 2006. Neural Variability in
583 Premotor Cortex Provides a Signature of Motor Preparation. *Journal of Neuroscience* 26, 3697–
584 3712. <https://doi.org/10.1523/JNEUROSCI.3762-05.2006>

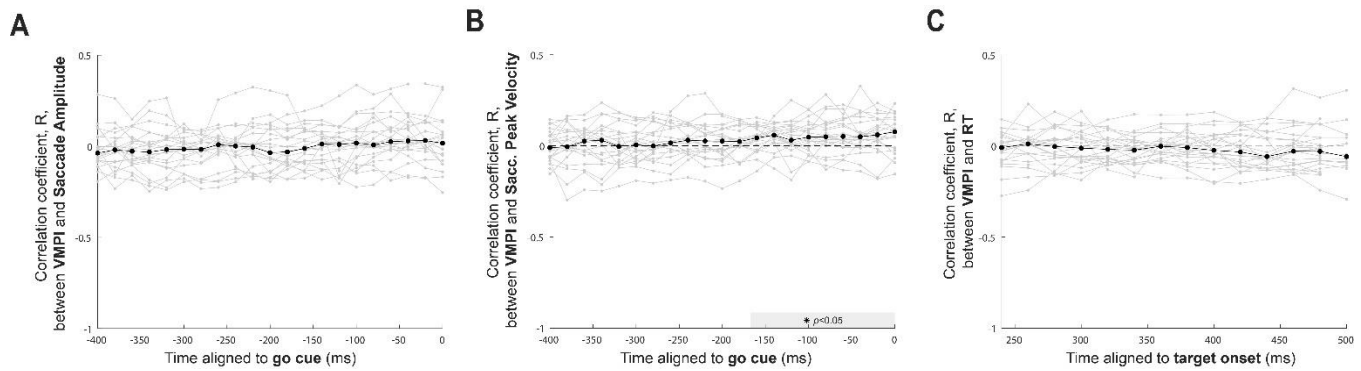
- 585 Cooper, B., McPeck, R.M., 2021. Role of the Superior Colliculus in Guiding Movements Not Made by
586 the Eyes. *Annual Review of Vision Science* 7, 279–300. <https://doi.org/10.1146/ANNUREV->
587 [VISION-012521-102314](https://doi.org/10.1146/ANNUREV-VISION-012521-102314)
- 588 Cowley, B.R., Kaufman, M.T., Butler, Z.S., Churchland, M.M., Ryu, S.I., Shenoy, K. v., Yu, B.M., 2013.
589 DataHigh: Graphical user interface for visualizing and interacting with high-dimensional neural
590 activity. *Journal of Neural Engineering* 10, 066012. <https://doi.org/10.1088/1741-2560/10/6/066012>
- 591 Cowley, B.R., Smith, M.A., Kohn, A., Yu, B.M., 2016. Stimulus-Driven Population Activity Patterns in
592 Macaque Primary Visual Cortex. *PLoS Computational Biology* 12, e1005185.
593 <https://doi.org/10.1371/JOURNAL.PCBI.1005185>
- 594 Cunningham, J.P., Yu, B.M., 2014. Dimensionality reduction for large-scale neural recordings. *Nature*
595 *Neuroscience* 17, 1500–1509. <https://doi.org/10.1038/nn.3776>
- 596 Darlington, T.R., Lisberger, S.G., 2020. Mechanisms that allow cortical preparatory activity without
597 inappropriate movement. *Elife* 9. <https://doi.org/10.7554/ELIFE.50962>
- 598 Dekleva, B.M., Kording, K.P., Miller, L.E., 2018. Single reach plans in dorsal premotor cortex during a
599 two-target task. *Nature Communications* 9, 1–12. <https://doi.org/10.1038/s41467-018-05959-y>
- 600 Gallego, J.A., Perich, M.G., Miller, L.E., Solla, S.A., 2017. Neural Manifolds for the Control of
601 Movement. *Neuron* 94, 978–984. <https://doi.org/10.1016/J.NEURON.2017.05.025>
- 602 Gandhi, N.J., Bonadonna, D.K., 2005. Temporal interactions of air-puff-evoked blinks and saccadic eye
603 movements: insights into motor preparation. *Journal of Neurophysiology* 93, 1718–1729.
604 <https://doi.org/10.1152/JN.00854.2004>
- 605 Gandhi, N.J., Katnani, H.A., 2011. Motor functions of the superior colliculus. *Annual Review of*
606 *Neuroscience* 34, 205–231. <https://doi.org/10.1146/ANNUREV-NEURO-061010-113728>
- 607 Gandhi, N.J., Keller, E.L., 1999. Comparison of saccades perturbed by stimulation of the rostral
608 superior colliculus, the caudal superior colliculus, and the omnipause neuron region. *Journal of*
609 *Neurophysiology* 82, 3236–3253. <https://doi.org/10.1152/JN.1999.82.6.3236>
- 610 Hafed, Z.M., 2021. Superior colliculus saccade motor bursts do not dictate movement kinematics.
611 *bioRxiv* 2021.06.24.449726. <https://doi.org/10.1101/2021.06.24.449726>
- 612 Hafed, Z.M., Chen, C.Y., Tian, X., 2015. Vision, perception, and attention through the lens of
613 microsaccades: Mechanisms and implications. *Frontiers in Systems Neuroscience* 9, 167.
614 <https://doi.org/10.3389/FNSYS.2015.00167/BIBTEX>
- 615 Hafed, Z.M., Krauzlis, R.J., 2010. Microsaccadic suppression of visual bursts in the primate superior
616 colliculus. *Journal of Neuroscience* 30, 9542–9547. <https://doi.org/10.1523/JNEUROSCI.1137->
617 [10.2010](https://doi.org/10.1523/JNEUROSCI.1137-10.2010)
- 618 Jagadisan, U.K., Gandhi, N.J., 2022. Population temporal structure supplements the rate code during
619 sensorimotor transformations. *Current Biology*. <https://doi.org/10.1016/J.CUB.2022.01.015>
- 620 Jagadisan, U.K., Gandhi, N.J., 2017. Removal of inhibition uncovers latent movement potential during
621 preparation. *Elife* 6. <https://doi.org/10.7554/ELIFE.29648>
- 622 Jagadisan, U.K., Gandhi, N.J., 2016. Disruption of Fixation Reveals Latent Sensorimotor Processes in
623 the Superior Colliculus. *Journal of Neuroscience* 36, 6129–6140.
624 <https://doi.org/10.1523/JNEUROSCI.3685-15.2016>

- 625 Jazayeri, M., Shadlen, M.N., 2010. Temporal context calibrates interval timing. *Nature Neuroscience*
626 13, 1020. <https://doi.org/10.1038/NN.2590>
- 627 Kaufman, M.T., Churchland, M.M., Ryu, S.I., Shenoy, K. v., 2015. Vacillation, indecision and hesitation
628 in moment-by-moment decoding of monkey motor cortex. *Elife* 4.
629 <https://doi.org/10.7554/ELIFE.04677>
- 630 Kaufman, M.T., Churchland, M.M., Ryu, S.I., Shenoy, K. v, 2014. Cortical activity in the null space:
631 permitting preparation without movement. *Nature Neuroscience* 17, 440–451.
632 <https://doi.org/10.1038/nn.3643>
- 633 Khademi, F., Chen, C.Y., Hafed, Z.M., 2020. Visual feature tuning of superior colliculus neural
634 reafferent responses after fixational microsaccades. *Journal of Neurophysiology* 123, 2136–2153.
635 <https://doi.org/10.1152/JN.00077.2020/>
- 636 Kobak, D., Brendel, W., Constantinidis, C., Feierstein, C.E., Kepecs, A., Mainen, Z.F., Qi, X.L., Romo,
637 R., Uchida, N., Machens, C.K., 2016. Demixed principal component analysis of neural population
638 data. *Elife* 5. <https://doi.org/10.7554/ELIFE.10989>
- 639 Latimer, K.W., Yates, J.L., Meister, M.L.R., Huk, A.C., Pillow, J.W., 2015. Single-trial spike trains in
640 parietal cortex reveal discrete steps during decision-making. *Science* (1979) 349, 184–187.
641 <https://doi.org/10.1126/science.aaa4056>
- 642 Lee, J., Groh, J.M., 2012. Auditory signals evolve from hybrid- to eye-centered coordinates in the
643 primate superior colliculus. *Journal of Neurophysiology* 108, 227–242.
644 <https://doi.org/10.1152/JN.00706.2011>
- 645 Leon, M.I., Shadlen, M.N., 2003. Representation of time by neurons in the posterior parietal cortex of
646 the macaque. *Neuron* 38, 317–327. [https://doi.org/10.1016/S0896-6273\(03\)00185-5](https://doi.org/10.1016/S0896-6273(03)00185-5)
- 647 Libby, A., Buschman, T.J., 2021. Rotational dynamics reduce interference between sensory and
648 memory representations. *Nature Neuroscience* 24, 715–726. [https://doi.org/10.1038/s41593-021-](https://doi.org/10.1038/s41593-021-00821-9)
649 [00821-9](https://doi.org/10.1038/s41593-021-00821-9)
- 650 Martinez-Conde, S., Macknik, S.L., Hubel, D.H., 2004. The role of fixational eye movements in visual
651 perception. *Nature Reviews Neuroscience* 5, 229–240. <https://doi.org/10.1038/nrn1348>
- 652 Massot, C., Jagadisan, U.K., Gandhi, N.J., 2019. Sensorimotor transformation elicits systematic
653 patterns of activity along the dorsoventral extent of the superior colliculus in the macaque monkey.
654 *Communications Biology* 2, 287. <https://doi.org/10.1038/S42003-019-0527-Y>
- 655 Miyashita, N., Hikosaka, O., 1996. Minimal synaptic delay in the saccadic output pathway of the
656 superior colliculus studied in awake monkey. *Experimental Brain Research* 112, 187–196.
657 <https://doi.org/10.1007/BF00227637>
- 658 Mullette-Gillman, O.A., Cohen, Y.E., Groh, J.M., 2005. Eye-centered, head-centered, and complex
659 coding of visual and auditory targets in the intraparietal sulcus. *Journal of Neurophysiology* 94,
660 2331–2352.
661 <https://doi.org/10.1152/JN.00021.2005/ASSET/IMAGES/LARGE/Z9K0080548220015.JPEG>
- 662 Peel, T.R., Hafed, Z.M., Dash, S., Lomber, S.G., Corneil, B.D., 2016. A Causal Role for the Cortical
663 Frontal Eye Fields in Microsaccade Deployment. *PLoS Biology* 14.
664 <https://doi.org/10.1371/JOURNAL.PBIO.1002531>

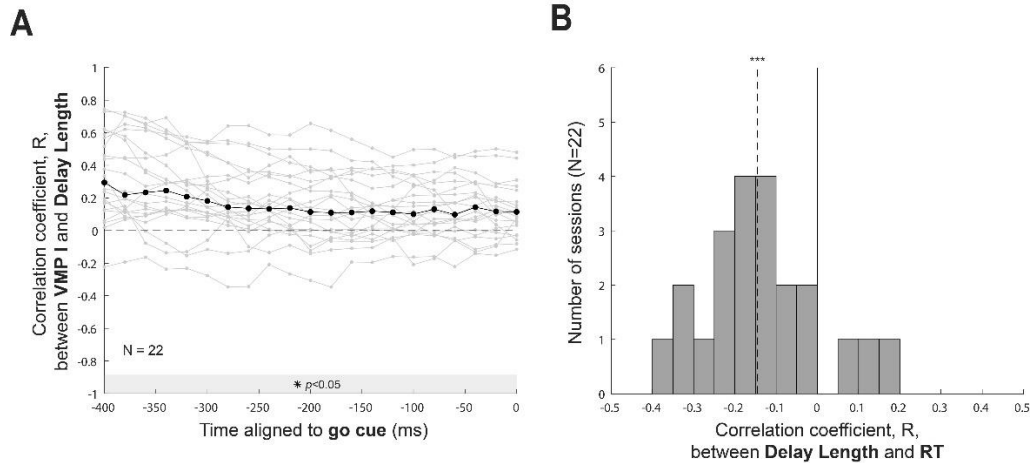
- 665 Robinson, D.L., Wurtz, R.H., 1976. Use of an extraretinal signal by monkey superior colliculus neurons
666 to distinguish real from self-induced stimulus movement. *Journal of Neurophysiology* 39, 852–870.
667 <https://doi.org/10.1152/JN.1976.39.4.852>
- 668 Sadeh, M., Sajad, A., Wang, H., Yan, X., Crawford, J.D., 2020. Timing Determines Tuning: A Rapid
669 Spatial Transformation in Superior Colliculus Neurons during Reactive Gaze Shifts. *eNeuro* 7.
670 <https://doi.org/10.1523/ENEURO.0359-18.2019>
- 671 Sajad, A., Sadeh, M., Crawford, J.D., 2020. Spatiotemporal transformations for gaze control.
672 *Physiological Reports* 8, e14533. <https://doi.org/10.14814/PHY2.14533>
- 673 Sajad, A., Sadeh, M., Yan, X., Wang, H., Crawford, J.D., 2016. Transition from Target to Gaze Coding
674 in Primate Frontal Eye Field during Memory Delay and Memory–Motor Transformation. *eNeuro* 3,
675 82. <https://doi.org/10.1523/ENEURO.0040-16.2016>
- 676 Semedo, J.D., Zandvakili, A., Machens, C.K., Yu, B.M., Kohn, A., 2019. Cortical Areas Interact through
677 a Communication Subspace. *Neuron* 102, 249-259.e4.
678 <https://doi.org/10.1016/J.NEURON.2019.01.026>
- 679 Shenoy, K. v, Sahani, M., Churchland, M.M., 2013. Cortical Control of Arm Movements: A Dynamical
680 Systems Perspective. *Annual Review of Neuroscience* 36, 337–359.
681 <https://doi.org/10.1146/annurev-neuro-062111-150509>
- 682 Smalianchuk, I., Jagadisan, U.K., Gandhi, N.J., 2018. Instantaneous Midbrain Control of Saccade
683 Velocity. *The Journal of Neuroscience* 38, 10156. [https://doi.org/10.1523/JNEUROSCI.0962-
684 18.2018](https://doi.org/10.1523/JNEUROSCI.0962-18.2018)
- 685 Tanaka, M., 2007. Cognitive Signals in the Primate Motor Thalamus Predict Saccade Timing. *Journal of*
686 *Neuroscience* 27, 12109–12118. <https://doi.org/10.1523/JNEUROSCI.1873-07.2007>
- 687 Trautmann, E.M., Stavisky, S.D., Lahiri, S., Ames, K.C., Kaufman, M.T., O’Shea, D.J., Vyas, S., Sun,
688 X., Ryu, S.I., Ganguli, S., Shenoy, K. v., 2019. Accurate Estimation of Neural Population Dynamics
689 without Spike Sorting. *Neuron* 103, 292-308.e4. <https://doi.org/10.1016/J.NEURON.2019.05.003>
- 690 Wurtz, R.H., Optican, L.M., 1994. Superior colliculus cell types and models of saccade generation.
691 *Current Ppinion in Neurobiology* 4, 857–861. [https://doi.org/10.1016/0959-4388\(94\)90134-1](https://doi.org/10.1016/0959-4388(94)90134-1)
- 692 Yu, B.M., Cunningham, J.P., Santhanam, G., Ryu, S.I., Shenoy, K. v., Sahani, M., 2009. Gaussian-
693 process factor analysis for low-dimensional single-trial analysis of neural population activity.
694 *Journal of Neurophysiology* 102, 614–635. <https://doi.org/10.1152/JN.90941.2008/>



Supplementary Figure 2. Single-trial delay period VMPI dynamics are highly variable. **A.** TOP: VMPI values on individual trials (gray) of an example session (same as [Figures 2, 4, and 6](#)) after removing trials in which a microsaccade was made during the delay period. The across-trial median trace is shown in black. All traces have been smoothed with a 5-point moving average filter. BOTTOM: Individual trials from the same example session, subsampled from the entire pool of no-microsaccade trials and individually colored to highlight the across-trial variability in the VMPI trace. **B.** Same as (A) but for a second example session. Here, the range of VMPI values around the across-trial median is much smaller, yet a similarly broad range of dynamics is observable in single trials.



Supplementary Figure 3. The relationship between VMPI and saccade metrics is variable. **A.** Across-session median correlation coefficient, R , between VMPI and saccade amplitude, for times leading up to the go cue. Same conventions as in Figure 7. There is never a significant correlation between the two variables (Wilcoxon signed rank test). **B.** Same as in (A) but for correlations between VMPI and single-trial peak velocity of the saccade. Time bins in which the median correlation coefficients were significantly different from zero ($p < 0.05$, Wilcoxon signed rank test) are shaded along the x axis in gray. A positive relationship between the two variables emerges approximately 160 ms before the go cue. **C.** Same as in Figure 7A but for correlations between the VMPI value aligned to the beginning of the delay period and single-trial RT. No significant correlations are observed (one-tailed Wilcoxon signed rank test).



Supplementary Figure 4. Delay lengths are correlated with both VMPI and RT. A. The VMPI value is significantly correlated with the delay period length even 400ms before each trial's go cue time ($p < 0.05$, Wilcoxon signed rank test). Same conventions as in Figure 7, with the across-session median correlation coefficients shown in black and individual sessions' correlation values shown in gray. **B.** Histogram of correlation values between each trial's delay period length and saccadic reaction time for the 22 sessions included in analysis of sensorimotor transformation. The across-session median correlation coefficient (-0.145) was significantly less than zero ($p < 0.0001$, one-tailed Wilcoxon signed rank test), indicating an inverse relationship between delay period length and reaction time.